Microelectronics Journal 147 (2024) 106166

Contents lists available at ScienceDirect

Microelectronics Journal

journal homepage: www.elsevier.com/locate/mejo

Evolutionary algorithm for minimizing the temperature influence of low power RF Energy Harvesting circuits☆

Renan Trevisoli [a,b,*], Lícia S.C. Lima [b], Humberto P. da Paz [b], Rodrigo T. Doria [c], Ivan R.S. Casella [b], Carlos E. Capovilla [b]

[a] Faculdade de Ciências Exatas e Tecnologia, Pontifícia Universidade Católica de São Paulo, R. Marquês de Paranaguá, 111, 01303-050, São Paulo, Brazil
[b] Centro de Engenharia, Modelagem e Ciências Sociais Aplicadas, Universidade Federal do ABC, Av. dos Estados, 5001, 09210-580, Santo André, Brazil
[c] Centro Universitário FEI, Av. Humberto de Alencar Castelo Branco, 3972, 09850-901, São Bernardo do Campo, Brazil

ARTICLE INFO

Keywords:
Energy Harvesting
Radio Frequency
Power efficiency
Evolutionary algorithm

ABSTRACT

The aim of this work is to analyze and optimize the design of low-power Radio Frequency (RF) Energy Harvesting rectifiers by using an Evolutionary Algorithm. Although, generally neglected in the literature, the RF rectifier operation strongly depends on the operation temperature. When it varies, the input impedance can change significantly, affecting the circuit matching and its power conversion efficiency. In this work, an evolutionary algorithm is used to identify which parameters of an RF diode are responsible for the performance degradation as a function of temperature and to optimize the rectifier circuit in order to reduce the temperature influence. This work demonstrates that the saturation current, the zero-bias junction capacitance, the load and the series resistance have an important impact in designing an optimized circuit. Results indicate that the applied algorithm can be used aiming the project of a circuit more robust to temperature variations. The obtained results have also been compared to experimental ones, corroborating the analysis.

1. Introduction

In the Internet of Things (IoT) era, low power wireless sensors are expected to be integrated into different environments, such as commercial, industrial, and personal. However, the energy storage systems of battery-powered wireless devices have a limited capacity, requiring constant recharges, and depending on the sensors location, the wired charge might not be accessible. For this reason, the Wireless Power Transfer (WPT) interest has increased in the academic community, aiming at the development of autonomous systems [1,2]. As Radio Frequency (RF) electromagnetic fields are commonly encountered in various environments due to the different wireless communication systems such as Wireless Fidelity (WiFi) and cellular networks, RF Energy Harvesting (RFEH) presents itself as a promising solution for powering wireless IoT devices [2–4]. However, one of the challenges for its full use is the low spectral power density of the most environments, which complicates its design [5–7].

The RF rectifier together with an antenna form a rectenna, which can be considered as the core of the RFEH circuit. The rectifier plays an important role in harvesting performance, and it usually uses Schottky diodes due to their low forward voltage drop, which increases the Power Conversion Efficiency (PCE), operating frequency range, and switching velocity [1]. However, the electrical behavior of diodes is significantly dependent on the operation temperature (T), such that a T increase reduces the forward voltage drop and increases the saturation current and the I–V curve slope [8]. This temperature-dependent behavior can affect the rectenna matching, reducing the power transfer and degrading the PCE, which can become a serious limitation for the low power RFEH, as demonstrated in [9], where the temperature dependent characteristics of commercial Schottky diodes are evaluated through their SPICE models. Therefore, the temperature influence on the rectifier should be carefully considered when designing RFEH systems that would operate in an environment whose temperature could vary. For instance, if the RFEH were applied to IoT devices to

☆ This work was supported in part by the Coordenação de Aperfeiçoamento de Pessoal de Nível Superior - Brazil (CAPES) - Finance Code 001; in part by Conselho Nacional de Desenvolvimento Científico e Tecnológico (CNPq) grants 309848/2018-0, 303938/2020-0, 406193/2022-3; in part by PUC-SP - PIPEq - AuxP under Grant 29509; and in part by Fundação de Amparo à Pesquisa do Estado de São Paulo (FAPESP) under Grant 2022/10876-0.

* Corresponding author at: Faculdade de Ciências Exatas e Tecnologia, Pontifícia Universidade Católica de São Paulo, R. Marquês de Paranaguá, 111, 01303-050, São Paulo, Brazil.

E-mail addresses: renan.trevisoli@ieee.org (R. Trevisoli), licia.lima@ufabc.edu.br (L.S.C. Lima), humberto.paz@ufabc.edu.br (H.P. da Paz), rtdoria@fei.edu.br (R.T. Doria), ivan.casella@ufabc.edu.br (I.R.S. Casella), carlos.capovilla@ufabc.edu.br (C.E. Capovilla).

https://doi.org/10.1016/j.mejo.2024.106166
Received 6 January 2024; Received in revised form 16 March 2024; Accepted 16 March 2024
Available online 18 March 2024
1879-2391/© 2024 Elsevier Ltd. All rights reserved.

sensor variables in an industrial or automotive environment, it would be subjected to temperature influence. Moreover, as circuits dissipate power when operating, their temperatures increase, also highlighting the temperature relevance On the other hand, determining the diode, whose PCE has the least dependence on T, can be a complex task, since it can depend, in addition to the T range, on the load (R_L) value.

Recently, there has been some effort to apply evolutionary computational techniques to the design of analog integrated circuits [10–14], generally focused on the design of amplifiers. Regarding the use of Evolutionary Algorithms (EA) in energy harvesting applications, there have been works related to different energy sources, such as piezoelectric [15,16], electromagnetic [17], and electromechanical [18]. Regarding RFEH, there are works related to optimizing the load and the microstrip size [19] and the antenna dimensions [20].

Although parameters in a design can be optimized by simply sweeping its values, such method can have limitations in the case of nonlinear components and when the influence of each parameter is not independent of the others. Aiming to provide a robust method for designing a series rectifier for RFEH, this work demonstrates the use of an EA for the determination of the desirable diode parameters focusing on a low T influence. Moreover, the algorithm has also been used to analyze each parameter influence aiming to clarify which are the most relevant ones in the tradeoff between T dependence and high PCE. To the best of our knowledge, the EA application aiming to determine the diode parameters that could minimize T influence on the PCE has not been addressed so far. It is important to comment that the series rectifier has been considered as one-diode topologies, which are indicated for low-power RFEH applications, due to their smaller losses [19,21,22].

The 2.4 GHz Industrial, Scientific and Medical (ISM) band, with a center frequency of 2.45 GHz [23] was been considered for the circuit analysis. Besides this introduction, Section 2 introduces the use of EAs, Section 3 describes the considered circuit, whereas Section 4 details the algorithm implementation. Sections 5 and 6 analyze the obtained results and compare them to experimental data, respectively. Finally, Section 7 highlights the conclusions of this work.

2. Evolutionary algorithm

EAs aim at mimicking natural selection, such that they can be used to optimize circuits by selecting the most appropriate ones and providing new generations of better circuits. Although evolution is a complex process consisting of numerous nonlinear interacting processes, its essence is based on variation and selection and can be represented through mapping functions that connect genetics with behavior [24].

The Genetic Algorithm (GA) is based on the chromosomes of living beings, which change their characteristics to survive in an environment [25]. Consequently, GA can be considered as an optimization method through stochastic search, developed to mimic the natural biological evolution and represented by operators such as selection, crossover, and mutation [25]. The concepts of GA can be applied to solve not only combinational optimization problems but also continuous [26] and multi-objective ones [27]. Besides that, GA has been shown to be efficient and stable in searching for global optimum solutions, mainly in complex and/or vast search space [28]. This is related to the dynamical changes through the search process and due to the evaluation of multiple individuals to produce multiple optimal solutions [29]. Moreover, GAs have excellent parallel capabilities, do not use derivatives [27,30], and do not require any prior knowledge about the objective function [31].

A flowchart of a GA [25] is presented in Fig. 1. At the beginning of the algorithm, the mutation rate, tolerance, population size, and parameters to be optimized are defined. In the sequence, an initial population is randomly created, and a fitness value is calculated for each member of the population. The next step corresponds to the selection. Just like natural selection acts on the organisms' behavior and is indirectly related to the genes [24], the circuit electrical behavior

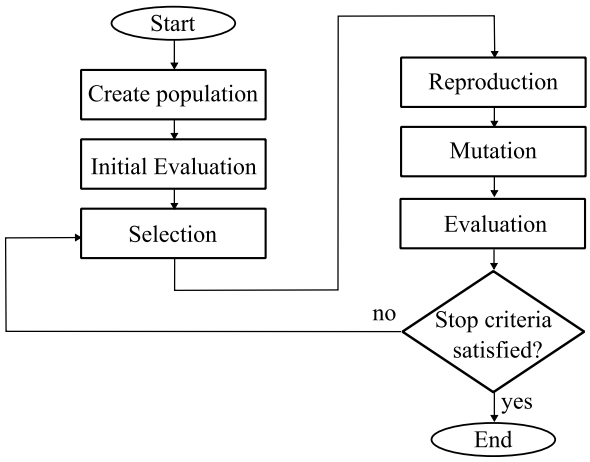

Fig. 1. Flowchart of the considered GA.

is used for the selection instead of the components' parameters. Then, the generation of a new population by crossover is performed, aiming at generating new chromosomes that retain only the good features [25]. To avoid getting stuck in a locally optimal area, mutation, which causes a random change in a gene, is applied [25]. These adaptations, based on selection, crossover, and mutation, occur in successive iterations through some generations [24], until a stop criterion is satisfied.

3. Circuit description

Among the existing rectifier topologies, the half wave is the simplest and has shown to be efficient for low power RFEH applications [21,22], such that it will be the focus of the current work. For such applications, Schottky diodes are commonly used, owing to their low forward voltage drop, operating frequency range, and fast switching capability [1].

Fig. 2 presents the rectifier block diagram at the top, which is composed of a matching network, a diode, an output low pass filter, and a load. Below in the same Figure, the schematic of the considered circuit based on the previous work of [32] is shown, where D represents the Schottky diode of the series rectifier. However, these diodes generally present low breakdown voltage (V_{BD}), such that they can conduct reversely even for relatively low reverse voltage (in the order of 2–3 V). This influence is considered by the diode D_r. The encapsulation of the components also includes the capacitive and inductive effects between pads, which are represented by C_p and L_p, respectively, and are related to parasitic effects. Additionally, the diode losses in the rectifier behavior are represented by the junction capacitance C_j and series resistance R_s of the diode. Therefore, the circuit shown inside the dashed rectangle represents the diode block. The low pass filter is composed of C_L in parallel with the load R_L. In the analysis of the rectifier, a voltage source applied directly to the diode block was considered. However, when analyzing the entire circuit, the corresponding matching network must also maximize the power transfer, as will be discussed in Section 6.

To analyze the circuit, an iterative procedure has been used, in which an initial input voltage (v_G) is applied to the circuit. In the sequence, following [32], the set of equations

$$\frac{di_G}{dt} = i_x \tag{1}$$

$$\frac{dv_L}{dt} = \frac{i_{CL}}{C_L} = \frac{1}{C_L}\left(i_G - \frac{v_L}{R_L}\right) \tag{2}$$

$$\frac{dv_D}{dt} = \frac{1}{R_S C_j}\left[v_G - L_P\, i_x - v_D - R_S(i_D - i_{Dr}) - v_L\right] \tag{3}$$

$$\frac{di_x}{dt} = \frac{1}{L_P C_P}\left[i_D - i_{Dr} - i_G + C_j\frac{dv_D}{dt} + C_P\left(\frac{dv_G}{dt} - \frac{dv_L}{dt}\right)\right] \tag{4}$$

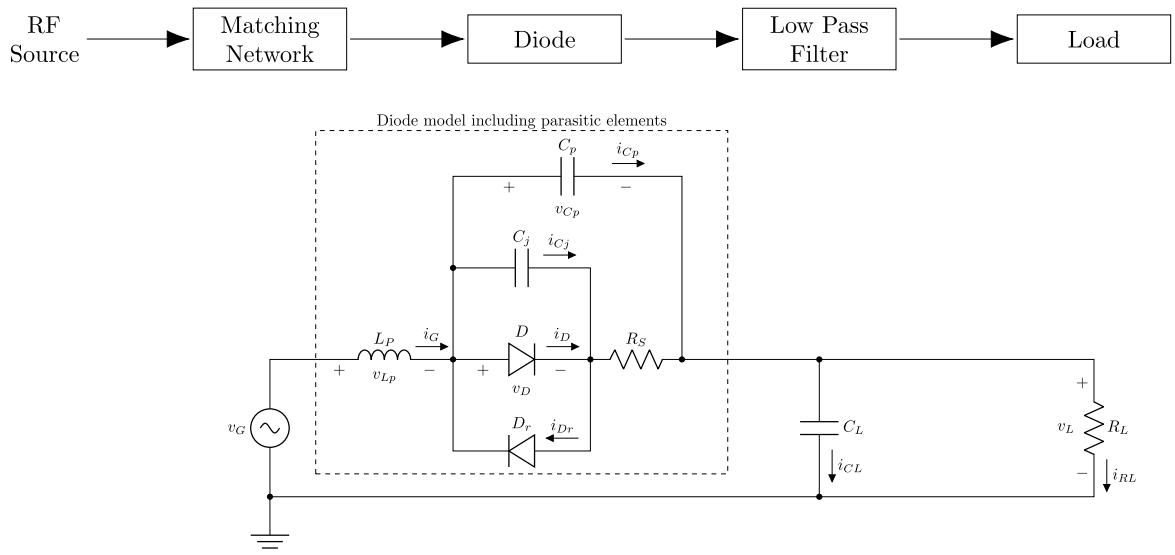

Fig. 2. Equivalent circuit for a packaged diode operating in a RF series rectifier.

can be solved to determine the load voltage (v_L) and the current supplied by the voltage source (i_G). The components and voltages used in (1)–(4) are indicated in Fig. 2. i_D and i_{Dr}, which are the direct and reverse diodes currents, respectively, are obtained by:

$$i_D = I_S \left[e^{\frac{v_D}{\eta V_t}} - 1 \right] \tag{5}$$

$$i_{Dr} = I_{BV} \left[e^{-\frac{(v_D - V_{BV})}{\eta_r V_t}} \right] \tag{6}$$

where I_S is the saturation current, I_{BV} is the current at the breakdown region, V_{BV} is the reverse breakdown voltage, η and η_r are the ideality factors for direct and reverse currents, respectively, $V_t = kT/q$ is the thermal voltage, q is the electron charge, k is the Boltzmann constant and T is the absolute temperature.

The input power (P_{in}) is obtained through the mean of the instant input power ($p_{in} = v_G i_G$). Since a fixed P_{in} has been considered, v_G is varied iteratively until the desired P_{in} is achieved. The output power (P_{out}) is calculated as the DC power at R_L. Consequently, the PCE is obtained through $PCE = \frac{P_{out}}{P_{in}}$. The rectifier complex input impedance (Z_{in}) can be obtained by the ratio of the source voltage to the fundamental component of the generator current, calculated using the Fast-Fourier Transform (FFT), following [1]. As the circuit is composed of capacitors and inductors, it has an implicit frequency (f) dependence. As the diode is a non-linear component and its electrical behavior is strongly dependent on T, both PCE and Z_{in} depend on P_{in}, frequency (f), and T [33,34].

4. Algorithm implementation

In this section, the GA implementation is explained, detailing how each of the flowchart steps shown in Fig. 1 has been considered. In this work, a real-coded GA has been considered, since its main advantages are robustness, efficiency, and accuracy [29].

4.1. Population creation

In the analysis performed, six diode parameters have been varied simultaneously in order to not only find the best configuration, but also identify which parameters most affect the rectifier temperature dependence. The parameters analyzed are I_S, R_S, the zero-bias junction capacitance (C_{j0}), the grading coefficient (M), the junction potential (V_j), and the load (R_L). It is worth noting that C_{j0}, M, and V_j are used to calculate C_j through:

$$C_j = C_{j0} \left(1 - \frac{v_D}{V_j} \right)^{-M} \tag{7}$$

Table 1
Limits of the diode parameters considered in this work.

Parameter	Limits	
	Minimum	Maximum
I_S [A]	$10^{-7.5}$	$10^{-4.0}$
R_S [Ω]	5.0	30.0
C_{j0} [pF]	0.1	0.2
M	0.3	0.5
V_j [V]	0.3	0.65
R_L [kΩ]	0.5	30.0

The population is composed of 30 devices and has been randomly populated considering the limits for each parameter as shown in Table 1. It is worth noting that the range for these parameters has been determined based on the ones exhibited by commercial devices. Except for I_S, a random uniform distribution between the limits has been considered. As I_S presents an exponential behavior, the random uniform distribution has been considered for its exponent (between −7.5 and −4.0) instead of its absolute value.

4.2. Evaluation

For each individual from the population, (1)–(4) are solved iteratively to obtain the PCE for a given P_{in}, which has been set to −20 dBm, a typical power magnitude for RFEH applications [9]. These equations consider the differential equations of the linear components together with the exponential equation of the diode to obtain the input impedance and the PCE for the nonlinear circuit considering the influence of the input power and temperature. The PCE is obtained for three different temperatures (260, 300, and 340 K), which cover the typical operating range of electronic devices. Two fitness functions have been analyzed separately, in order to verify which would be more adequate:

$$f_1 = \frac{1}{n} \sum_{i=1}^{n} PCE_i, \tag{8}$$

where n is the number of temperatures considered, $i = 1$, 2 and 3 represent $T = 260$, 300 and 340 K, respectively, such that f_1 represents

the mean PCE obtained for all T and

$$f_2 = \frac{PCE_{min}^2}{\sqrt{\frac{\sum_{i=1}^{n} |PCE_i - f_1|^2}{n}}}, \quad (9)$$

where PCE_{min} represents the minimum PCE for the analyzed T. This latter fitness function represents the PCE normalized by its standard deviation aiming to obtain the highest efficiency with a minimum dependence on T.

4.3. Selection and reproduction

After calculating the fitness of every individual in a generation, the population is ordered in descending order and a probability is assigned for each individual following (10), such that the ones with the highest fitness have the highest probability of reproducing.

$$p_i = \frac{[(n+1) - i]^k}{\sum_{i=1}^{n} [(n+1) - i]^k} \quad (10)$$

where k is used to control the algorithm convergence. Its influence is analyzed in Section 5.2.

The reproduction is performed by selecting two individuals from the population considering the non-uniform probability. Next, each out of the six parameters is selected randomly either from the first or from the second individual, creating a new one that is a combination of both. This procedure is repeated until a new population is obtained.

4.4. Mutation

Mutation aims at preventing the algorithm to get stuck in a local maxima area. Therefore, it is characterized by a stochastic change in the parameter different from its parent values. To perform it, a mutation probability of 0.1 has been considered, meaning that each parameter of each individual has a 10% probability of suffering mutation. If it occurs, the parameter value is changed to ±50% of its anterior value, which is also defined randomly. The limits shown in Table 1 have been considered as hard limits, such that if the mutated value falls out of its permitted range, the parameter has been redefined to its closest boundary.

4.5. Stop criteria

Two stop criteria have been considered in the algorithm implementation: number of generations and fitness tolerance. It firstly should be pointed out that the diode parameters are continuous whereas the population is formed by discrete values of these parameters. Consequently, the best solution inside the set of discrete values does not necessarily correspond to the optimal global values for the device. Therefore, intensification inside the promising area [26], which reduces the search domain around the best point found in the last generation, can be applied. It reduces the neighborhood of individuals and generates another population inside the new search domain [26], in a similar way to the generation of the initial population. In this work, a total of 25 generations for the parameters optimization has been considered, in which 5 generations were considered before an intensification process has been applied. Therefore, 4 intensifications inside the promising area were performed aiming to reach the globally optimal values. For each intensification, a higher reduction in the search domain is considered to provide a fine search for the optimal parameters set.

Besides the number of generations, a fitness tolerance parameter has been defined aiming to avoid unnecessary calculations when the parameters get stuck in a local or global maximum. If the change between the fitness function results considering two adjacent generations has been lower than the tolerance, the next intensification step is anticipated. In this work, the tolerance has been set to 1 in both f_1 and f_2 fitness functions. As f_1 represents a percentage, the considered tolerance means a variation lower than 1% of PCE when T is varied. f_2 presents a higher value, since PCE is squared in its calculation, as will be shown in Section 5.1, such that the obtained fitness value remains practically unchanged between two adjacent generations. Table 2 summarizes the parameters considered in the algorithm implementation. It should be mentioned that the parameters were adjusted based on extensive testing of the algorithm to achieve a compromise between convergence and time of simulation.

Table 2
Parameters considered in the algorithm implementation.

Parameter	Value
Population size in each generation	30
Mutation probability	0.1
Total number of generations	25
Number of generations before intensification	5
Tolerance in fitness functions	1

5. Results and discussions

This Section analyzes the results of the implemented algorithm as well as the device selected by the GA.

5.1. Fitness function

In the first analysis, a comparison between the results obtained through the two fitness functions described in Section 4.2 has been performed. Fig. 3 presents the values using f_1 and f_2 obtained along different generations. The two functions were calculated for all generations, however, only one of the functions was used to control the algorithm evolution. The cross symbols indicate the cases when f_1 was used to control the evolution, whereas the circles indicate the use of f_2. The red and blue curves represent two optimization processes considering different initial populations (seeds #1 and #2). As can be observed, the evolution of both fitness functions has shown to be independent of the initial population, as desired. When comparing the results of the functions, although both lead to similar f_1 results, a smaller dependence on the temperature is expected when f_2 is used to control the evolution, which can be seen by the higher f_2 values in Fig. 3 (right).

5.2. Analysis of the selection procedure

In this Section, the influence of the parameter k in (10) is presented. In Fig. 4, the results of the fitness functions f_1 (left) and f_2 (center) are exhibited along the generations for six different cases, varying the value of the parameter k. The results show that k affects the speed of convergence of the algorithm along the generations as well as the final f_1 and f_2 values. A low k value reduces the difference between the probabilities of each individual of being selected for reproduction. Therefore, the dominant characteristics are not efficiently passed through the generations, delaying evolution, such that f_2 has been significantly lower for $k = 1$, 2, and 3. On the other hand, for the highest k considered, f_2 has also been significantly low. In this case, only the first individuals are selected, reducing the diversity and, consequently, harming the evolution of the characteristics. Following the data of Fig. 4 (right), which shows f_2 for the last generation as a function of k, it has been set to 4.

5.3. Selected devices

The diode parameters obtained for the four optimization processes of Fig. 3 are summarized in Table 3. Two processes with a different initial population (seeds) have used each fitness function (either f_1 or f_2) to control the evolution. Both functions have led to similar

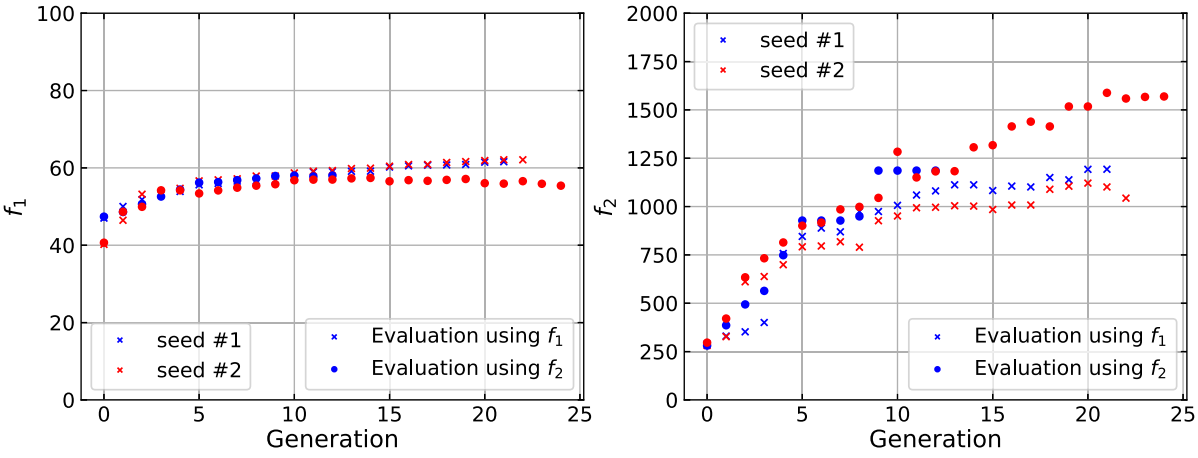

Fig. 3. f_1 (left) and f_2 (right) along the different generations considering the different fitness functions.

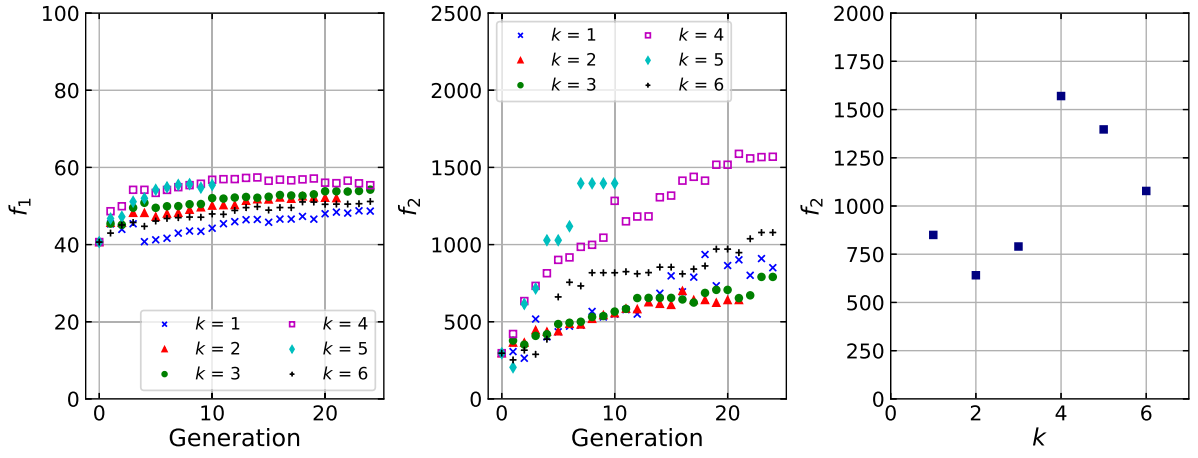

Fig. 4. f_1 (left) and f_2 (center) along the different generations considering the different k values, and f_2 at the last generation as a function of k (right).

Table 3
Diode parameters obtained for the four optimization processes of Fig. 3.

Parameter	Fitness function used			
	f_1		f_2	
	seed #1	seed #2	seed #1	seed #2
I_S [A]	$10^{-7.24}$	$10^{-7.08}$	$10^{-6.89}$	$10^{-7.07}$
R_S [Ω]	4.0	3.9	5.4	5.3
C_{j0} [pF]	0.080	0.078	0.086	0.108
M	0.36	0.51	0.37	0.49
V_j [V]	0.36	0.47	0.31	0.31
R_L [kΩ]	37.4	34.6	29.8	35.8

diode parameters. Some of the values in Table 3 are outside the range of Table 1. Although the latter was considered a hard limit for the case of mutation, the intensification process, which reduced the search domain, could slightly increase the parameters ranges.

To further analyze the results, the parameters obtained through f_2 seed #1 were selected, and the electrical behavior of the diode with such parameters has been obtained through the solution of (1)–(4). To analyze the diode operation at a different condition from the fixed input power considered during the optimization process, Fig. 5 (left) presents the PCE results as a function of P_{in} for different T. PCE remains between 53 and 60% for the entire analyzed T range at $P_{in} = -20$ dBm. It can be noted that T influence is reduced when increasing P_{in}, until reverse conduction degrades PCE. This small PCE dependence on T is significantly lower than the ones generally observed in commercial devices, as shown in [9]. At Fig. 5 (right), PCE is shown as a function of P_{in} for the best diode obtained at the end of the first generation. The mean PCE among the analyzed T is about 57 and 44% at $P_{in} = -20$ dBm for the last and first generations, respectively. The PCE variation with T for the same P_{in} has reduced from 10 to 7% between the same generations. These results indicate that the parameters set has adequately evolved.

In Fig. 6, the components of the complex rectifier input impedance are shown as a function of P_{in}. The variation of Z_{in} with T can significantly affect the power transfer from the antenna to the load, since the Matching Network (MN), which is important to maximize the power transfer [35], would not be matched for all T. Its resistive part (R_{in}) has demonstrated a low dependence on T for the analyzed range, as shown in Fig. 6 (left). At $P_{in} = -20$ dBm, the curves for different T are crossing leading to a point with no T dependence. The reactive part of Z_{in} (X_{in}) has shown a higher dependence on T than R_{in}. However, this dependence is still lower than that of the commercial diode SMS7630-079LF as presented in [9].

5.4. Determining each parameter influence

In the sequence, a deeper analysis of the influence of each parameter of the circuit dependence on T has been carried out. For that, the PCE curves of the rectifier have been obtained varying one parameter at a time, while maintaining the others fixed in the values of Table 3. Fig. 7 presents the PCE as a function of P_{in} considering the variation of either I_S (left) or R_L (right) while other parameters have been kept fixed. To facilitate the visualization, each color represents one temperature, whereas each symbol is related to I_S or R_L. It can be seen that I_S

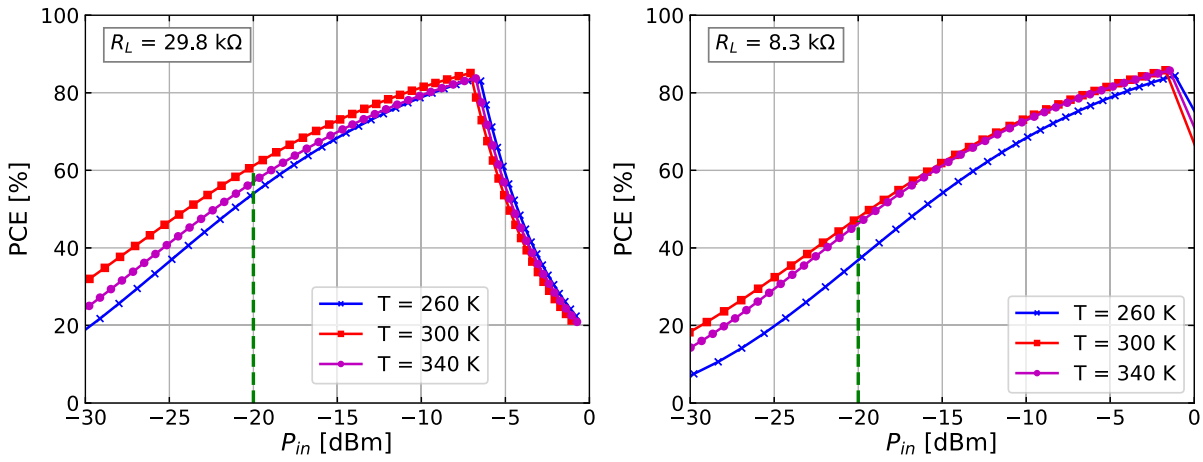

Fig. 5. PCE for different temperatures as a function of P_{in} for the diode with the characteristics determined by the GA at the end of the optimization process (left) and at the end of the first generation (right).

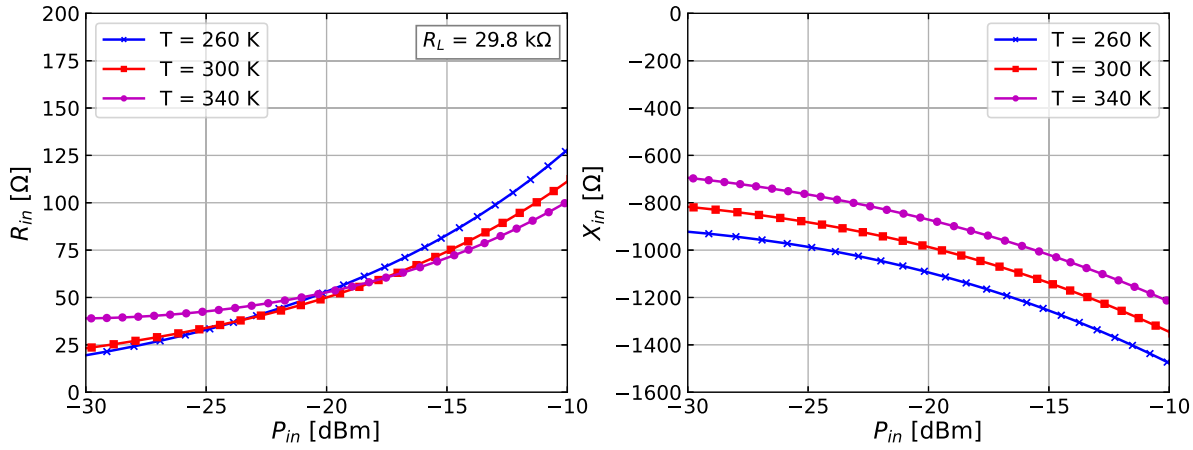

Fig. 6. The real (left) and imaginary (right) components of Z_{in} for different temperatures as a function of P_{in} for the diode with the characteristics determined by the GA.

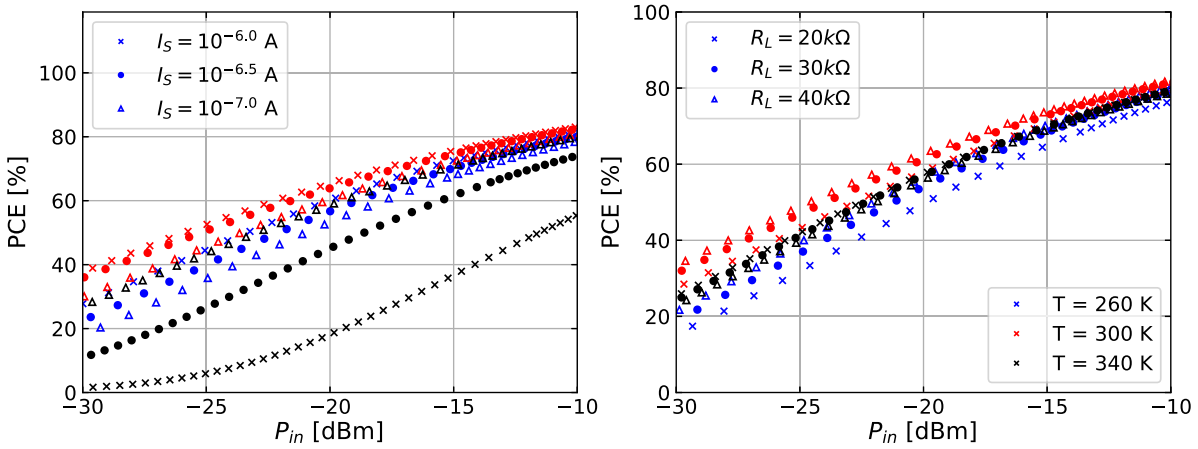

Fig. 7. PCE as a function of P_{in} varying only I_S (left) and R_L (right) for different temperatures while maintaining the other parameters fixed.

significantly affects the dependence of the PCE on the temperature, especially for the higher currents. Regarding R_L, it has not shown to influence significantly the dependence of PCE on T for higher P_{in}. For lower P_{in}, the influence of R_L on both the efficiency and its dependence on T increases, where a higher R_L seems to provide higher efficiency.

In Fig. 8, the influences of C_j and R_s are analyzed. These parameters should be kept as low as possible in order to maximize the PCE, as expected, since they are related to parasitic components in the rectifier. Moreover, the variation of any of them does not seem to affect the T influence on PCE. The last two parameters (V_j and M) influences are presented in Fig. 9 (left) and (right), respectively. Their values do not alter the PCE dependence on T.

Finally, Fig. 10 shows the histogram of the studied parameters from the last population used in the optimization process that considered f_2 as the evolution control and seed #1 for the initial population. Similarly to Fig. 8, the last population is composed of devices with reduced C_j

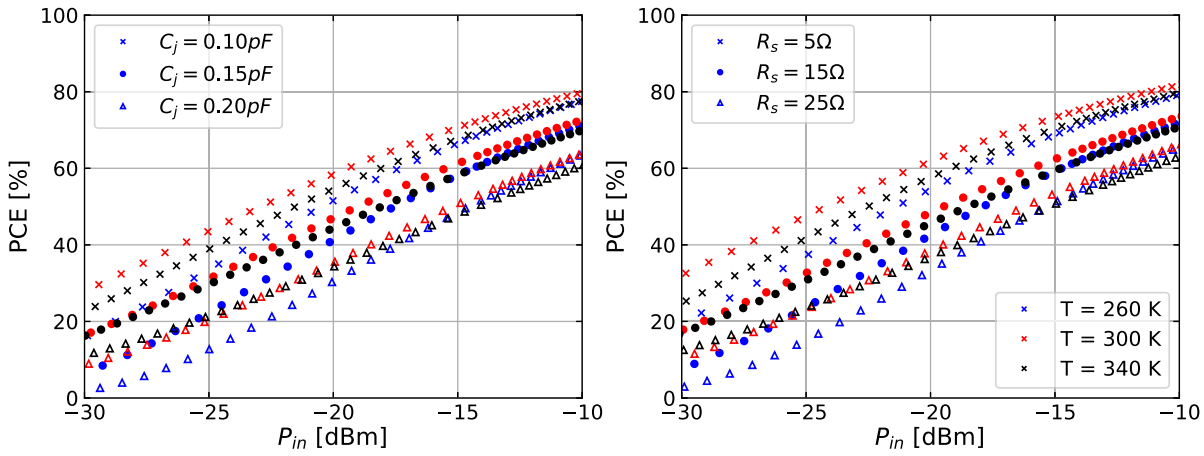

Fig. 8. PCE as a function of P_{in} varying only C_j (left) and R_s (right) for different temperatures while maintaining the other parameters fixed.

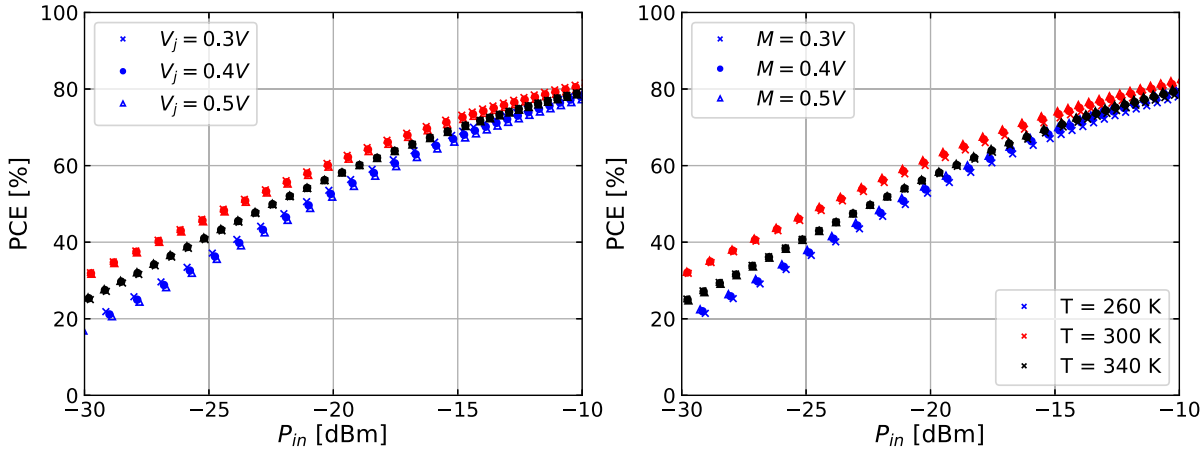

Fig. 9. PCE as a function of P_{in} varying only V_j (left) and M (right) for different temperatures while maintaining the other parameters fixed.

and R_s, since the lower these values, the higher the PCE. Although V_j and M have shown to not affect the rectifier dependence on T in Fig. 9, they have also converged towards their lower limit values. I_S and R_L have converged towards a low saturation current and a high load resistance, aiming to reduce the temperature influence.

6. Comparison to practical rectifier evaluation

The data shown in Section 5 considered the maximum theoretical PCE that could be reached for each P_{in} for a specific diode. To maximize the power transfer from the antenna to the rectifier, an MN is added to the circuit. To include its influence on the analysis, the same procedure of [32] has been considered. Z_{in} for the reference condition (T = 300 K and P_{in} = −20 dBm) is initially obtained and the rectifier reflection coefficient (Γ_{ret}) is calculated. Then, the ideal impedance MN S-parameters for the reference condition are determined considering $S_{11} = S_{22} = \Gamma_{ret}^*$, where Γ_{ret}^* is the reflection coefficient conjugate, S_{12} and S_{21} are calculated considering a lossless line. For a reciprocal two-port network with a zero reflection coefficient at the source, the two-port network gain (G) is given by (11) [36], which should multiply PCE for the MN influence inclusion on the rectifier efficiency.

$$G = \frac{(1 - |\Gamma_{ret}|^2)|S_{21}|^2}{|(1 - \Gamma_{ret} S_{22})|^2} \tag{11}$$

Table 4 presents the parameters of commercial diodes used in RFEH. Comparing them with the results analyzed in Section 5, such as those summarized in Fig. 10, it can be concluded that the diode SMS7621 is expected to present a lower dependence on T, due to the I_S closer to the value of Table 3, lower C_{j0}, and relatively low R_s.

Table 4
Parameters of common diodes used in RFEH.

Parameter	Commercial diodes			
	SMS7630	SMS7621	HSMS285x	HSMS286x
I_S [A]	5×10^{-6}	4×10^{-8}	3×10^{-6}	5×10^{-8}
R_S [Ω]	20	12	25	6
C_{j0} [pF]	0.14	0.10	0.18	0.18
M	0.40	0.35	0.50	0.50
V_j [V]	0.34	0.51	0.35	0.65

Fig. 11 exhibits the modulus of the reflection coefficient of the rectifier as a function of f considering the use of a diode with the optimized parameters (solid lines), and the commercial diode SMS7621-079LF (dashed lines). In this case, the coefficient is obtained considering the influence of a lossless MN, calculated using (11). The SMS7621 diode has demonstrated a lower dependence of the central frequency on T than the diode with the optimized parameters, since the optimization process has focused on the PCE and its dependence on T. Also, in the figure, the experimental data of the rectifier analyzed in [9] obtained at room temperature ($T \approx 300$ K) is presented for comparison purposes. The substrate used in the prototype is a low cost FR-4 (ϵ_r = 4.5), with thickness of 1.6 mm and $\tan(\delta)$ = 0.02. The MN was designed using a T-type filter with three low-losses inductors, whose values were calculated based on the Z_{in} analysis. Further details of the prototype

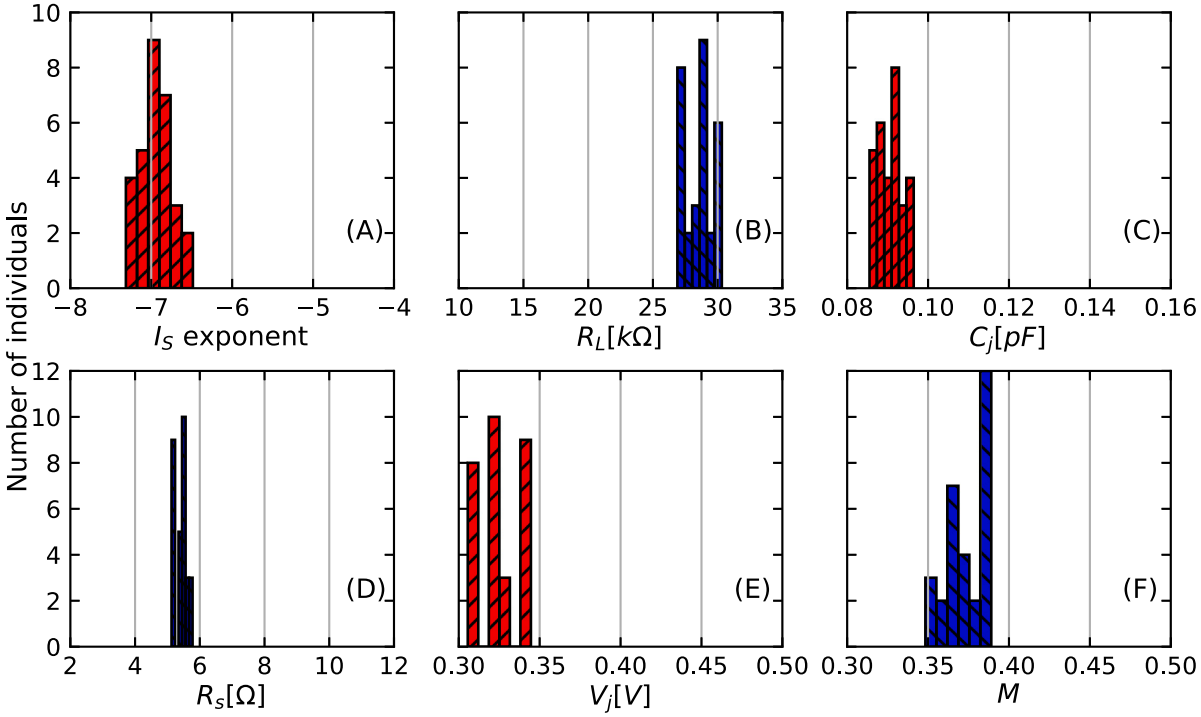

Fig. 10. Histogram of the parameters I_S exponent (A), R_L (B), C_j (C), R_s (D), V_j (E), M (F) of the last population used in the optimization process.

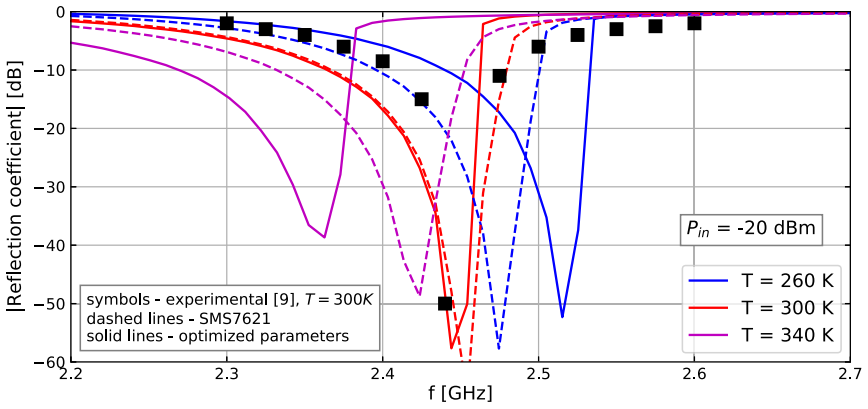

Fig. 11. Modulus of the reflection coefficient as a function of f for the simulated rectifier with the optimized and SMS7621 diodes, together with experimental data of [9].

can be found in [9]. The simulated results present similar behavior to the experimental ones.

Finally, PCE is shown as a function of the temperature at 2.45 GHz in Fig. 12 for the diodes SMS7621, SMS7630, and the one with optimized parameters, whose values were obtained using the fitness function f_2 considering seed #1 as shown in Table 3. The curves are exhibited for different P_{in}. Solid and dashed lines indicate the PCE considering and neglecting the MN influence, respectively. Although PCE presents a small dependence on T for both SMS7621 and optimized diodes, the MN increases significantly this dependence, as the circuit would not be matched for all T. For the SMS7630, a significant decrease in PCE is observed at higher temperatures for all P_{in}, which is in accordance with the analysis of Section 5.3. In the figure, the experimental data of [9] for $P_{in} = -20$ dBm is also shown for comparison purposes for the diodes SMS7621 and SMS7630. For the former, PCE is significantly lower than its maximum theoretical value indicated by the lines, which can be related to losses and small mismatches in the MN [9]. For the latter, the obtained PCE is closer to the predicted, showing a higher dependence on T, owing mainly to the higher I_S.

7. Conclusions

This work proposed the use of an evolutionary algorithm to optimize the design of RFEH rectifiers. As the electrical behavior of such circuits is generally strongly dependent on the operation temperature, the identification of the characteristics that could reduce this influence might be of interest to projecting more robust circuits. The algorithm has been based on a previous developed analytical model for series rectifiers and has been used not only to determine the characteristics of the most adequate device, but also to analyze the cross-relation of each considered parameter and T. The optimized parameters could be used either to select the diode off-the-shelf or to guide the fabrication of a customized diode for the RFEH circuit. In both cases, if not all the characteristics can be reached, the algorithm helps in understanding which parameters are the most relevant for a robust circuit design, defining the primary characteristics that should be met. Results have shown that the diode saturation current has a significant impact on the rectifier efficiency dependence on T, the junction capacitance and series resistance play a significant role in increasing the PCE, whereas

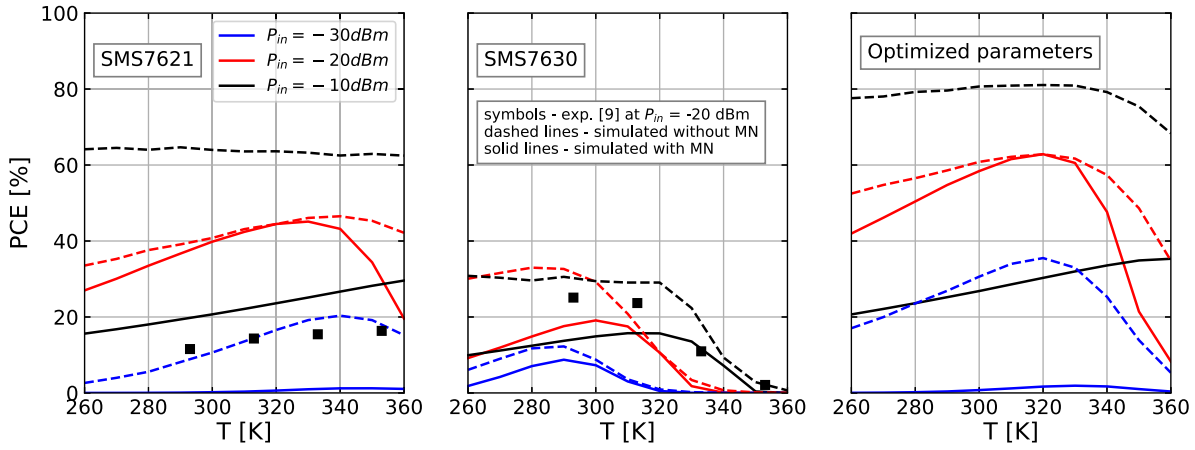

Fig. 12. PCE as a function of T for different P_{in} and f = 2.45 GHz for the diodes: SMS7621 (left), SMS7630 (center), and optimized parameters (right). The solid and dashed lines represent PCE considering and neglecting the MN, respectively. The symbols are the experimental data of [9] for P_{in} = −20 dBm.

the load resistance demonstrated a moderate influence on PCE and its dependence on T. Experimental measurements also corroborate the results obtained in the performance analyzes carried out.

CRediT authorship contribution statement

Renan Trevisoli: Conceptualization, Methodology, Software, Formal analysis, Writing - original draft, Visualization, Funding acquisition. **Lícia S.C. Lima:** Formal analysis, Writing – review & editing, Visualization. **Humberto P. da Paz:** Investigation, Data curation, Writing – review & editing. **Rodrigo T. Doria:** Conceptualization, Formal analysis, Writing – review & editing, Funding acquisition. **Ivan R.S. Casella:** Validation, Formal analysis, Writing – review & editing. **Carlos E. Capovilla:** Validation, Formal analysis, Writing – review & editing, Supervision, Funding acquisition.

Declaration of competing interest

The authors declare the following financial interests/personal relationships which may be considered as potential competing interests: Rodrigo T. Doria, Carlos E. Capovilla reports financial support was provided by National Council for Scientific and Technological Development. Carlos E. Capovilla, Renan Trevisoli reports financial support was provided by State of Sao Paulo Research Foundation. If there are other authors, they declare that they have no known competing financial interests or personal relationships that could have appeared to influence the work reported in this paper.

Data availability

Data will be made available on request.

References

[1] S. Nikoletseas, Y. Yang, A. Georgiadis, Wireless Power Transfer Algorithms, Technologies and Applications in Ad Hoc Communication Networks, Springer, 2016.

[2] D.W.K. Ng, T.Q. Duong, C. Zhong, R. Schober, Wireless Information and Power Transfer: Theory and Practice, John Wiley & Sons, 2019.

[3] A.A. Helaly, A.N. Mohieldin, An integrated thermal and RF energy harvesting system with rectifying combination and storage controller for IoT devices, Microelectron. J. 142 (2023) 106020.

[4] Y. Tian, L. Liu, J. Ma, A high-sensitivity, low-noise dual-band RF energy harvesting and managing system for wireless bio-potential acquisition, Microelectron. J. 116 (2021) 105239.

[5] N.B. Carvalho, A. Georgiadis, Wireless Power Transmission for Sustainable Electronics: COST WiPE-IC1301, John Wiley & Sons, 2020.

[6] S. Kim, R. Vyas, J. Bito, K. Niotaki, A. Collado, A. Georgiadis, M.M. Tentzeris, Ambient RF energy-harvesting technologies for self-sustainable standalone wireless sensor platforms, Proc. IEEE 102 (11) (2014) 1649–1666.

[7] Y. Luo, L. Pu, Practical issues of RF energy harvest and data transmission in renewable radio energy powered IoT, IEEE Trans. Sustain. Comput. 6 (4) (2020) 667–678.

[8] S. Sze, K.K. Ng, Physics of Semiconductor Devices, Wiley, 2007.

[9] H.P.D. Paz, V.S.D. Silva, R. Diniz, R. Trevisoli, C.E. Capovilla, I.R.S. Casella, Temperature analysis of schottky diodes rectifiers for low-power RF energy harvesting applications, IEEE Access 11 (2023) 54122–54132.

[10] M.F. Barros, J.M. Guilherme, N.C. Horta, Analog circuits and systems optimization based on evolutionary computation techniques, Vol. 9, Springer, 2010.

[11] R.A. de Lima Moreto, C.E. Thomaz, S.P. Gimenez, Gaussian fitness functions for optimizing analog CMOS integrated circuits, IEEE Trans. Comput.-Aided Des. Integr. Circuits Syst. 36 (10) (2017) 1620–1632.

[12] L.C. Severo, D. Longaretti, A. Girardi, Simulation-based evolutionary heuristic to sizing an OTA Miller with design centering analysis, in: 2012 Argentine School of Micro-Nanoelectronics, Technology and Applications, EAMTA, IEEE, 2012, pp. 111–115.

[13] A. Jafari, E. Bijami, H.R. Bana, S. Sadri, A design automation system for CMOS analog integrated circuits using new hybrid shuffled frog leaping algorithm, Microelectron. J. 43 (11) (2012) 908–915.

[14] P.-C. Pan, H.-M. Chen, C.-C. Lin, et al., PAGE: parallel agile genetic exploration towards utmost performance for analog circuit design, in: DATE, 2013, pp. 1849–1854.

[15] S. Bagheri, N. Wu, S. Filizadeh, Application of artificial intelligence and evolutionary algorithms in simulation-based optimal design of a piezoelectric energy harvester, Smart Mater. Struct. 29 (10) (2020) 105004.

[16] M. Yadav, D. Yadav, R.K. Garg, R.K. Gupta, S. Kumar, D. Chhabra, Modeling and optimization of piezoelectric energy harvesting system under dynamic loading, in: Advances in Fluid and Thermal Engineering: Select Proceedings of FLAME 2020, Springer, 2021, pp. 339–353.

[17] B. Yan, S. Zhou, C. Zhao, K. Wang, C. Wu, Electromagnetic energy harvester for vibration control of space rack: modeling, optimization, and analysis, J. Aerosp. Eng. 32 (1) (2019) 04018126.

[18] D. Sequeira, K. Coonley, B. Mann, Topological optimization of variable area plate capacitors for coupled electromechanical energy harvesters, J. Intell. Mater. Syst. Struct. 30 (15) (2019) 2198–2211.

[19] R.L.R.d. Silva, S.T.M. Gonçalves, C. Vollaire, A. Bréard, G.L. Ramos, C.G.d. Rego, Analysis and optimization of ultra-low-power rectifier with high efficiency for applications in wireless power transmission and energy harvesting, J. Microw. Optoelectron. Electromagn. Appl. 19 (1) (2020) 60–85.

[20] M.C. Derbal, M. Nedil, A high gain dual band rectenna for RF energy harvesting applications, Progr. Electromagnet. Res. Lett. 90 (2020) 29–36.

[21] H.P. Paz, V.S. Silva, E.V. Cambero, H.X. Araújo, I.R. Casella, C.E. Capovilla, A survey on low power RF rectifiers efficiency for low cost energy harvesting applications, AEU - Int. J. Electr. Commun. 112 (2019) 152963.

[22] Y.-S. Chen, C.-W. Chiu, Theoretical limits of rectifying efficiency for low-power wireless power transfer, Int. J. RF Microw. Comput.-Aided Eng. 28 (4) (2018) e21218.

[23] G.C. Garcia, R. Vargas, J.D. Melo, I.R.S. Casella, Analysis of the optimized allocation of wireless and PLC data concentrators in extensive low-voltage networks considering the increase in the residential electric vehicles charging, IEEE Access 11 (2023) 140774–140788, http://dx.doi.org/10.1109/ACCESS.2023.3339563.

[24] J.M. Keller, D. Liu, D.B. Fogel, Fundamentals of Computational Intelligence: Neural Networks, Fuzzy Systems, and Evolutionary Computation, John Wiley & Sons, 2016.
[25] C.-H. Chen, D.S. Naidu, Fusion of Hard and Soft Control Strategies for the Robotic Hand, John Wiley & Sons, 2017.
[26] R. Chelouah, P. Siarry, A continuous genetic algorithm designed for the global optimization of multimodal functions, J. Heuristics 6 (2000) 191–213.
[27] M. Gendreau, J.-Y. Potvin, Handbook of Metaheuristics, second ed., Springer New York, NY, 2009.
[28] K. Dasgupta, B. Mandal, P. Dutta, J.K. Mandal, S. Dam, A genetic algorithm (GA) based load balancing strategy for cloud computing, Proc. Technol. 10 (2013) 340–347, First International Conference on Computational Intelligence: Modeling Techniques and Applications (CIMTA) 2013.
[29] S. Katoch, S.S. Chauhan, V. Kumar, A review on genetic algorithm: past, present, and future, Multimedia Tools Appl. 80 (2021) 8091–8126.
[30] X. Lü, Y. Wu, J. Lian, Y. Zhang, C. Chen, P. Wang, L. Meng, Energy management of hybrid electric vehicles: A review of energy optimization of fuel cell hybrid power system based on genetic algorithm, Energy Convers. Manage. 205 (2020) 112474.
[31] G. Papazoglou, P. Biskas, Review and comparison of genetic algorithm and particle swarm optimization in the optimal power flow problem, Energies 16 (3) (2023).
[32] R. Trevisoli, H.P.d. Paz, V.S.d. Silva, R.T. Doria, I.R.S. Casella, C.E. Capovilla, Modeling schottky diode rectifiers considering the reverse conduction for RF wireless power transfer, IEEE Trans. Circuits Syst. II 69 (3) (2022) 1732–1736.
[33] S. Shieh, M. Kamarei, Transient input impedance modeling of rectifiers for RF energy harvesting applications, IEEE Trans. Circuits Syst. II 65 (3) (2018) 311–315.
[34] J.-h. Ou, S.Y. Zheng, A.S. Andrenko, Y. Li, H.-Z. Tan, Novel time-domain schottky diode modeling for microwave rectifier designs, IEEE Trans. Circuits Syst. I. Regul. Pap. 65 (4) (2018) 1234–1244.
[35] E.V.V. Cambero, H.P. da Paz, V.S. da Silva, D. Consonni, C.E. Capovilla, I.R.S. Casella, A revised methodology to analyze the rectenna power conversion efficiency based on antenna/rectifier interface losses, AEU - Int. J. Electr. Commun. 134 (2021) 153686.
[36] R.E. Collin, Foundations for Microwave Engineering, second ed., John Wiley & Sons, 2001.